ELSEVIER

Journal of Power Sources 91 (2000) 99–106

JOURNAL OF POWER SOURCES

www.elsevier.com/locate/jpowsour

Effect of geometrical variations on AMTEC cell heat losses

M.A.K. Lodhi *, A. Daloglu [1]

Department of Physics, Texas Tech. University, Box 41051, Lubbock, TX 79409-1051, USA

Received 23 November 1999; accepted 16 February 2000

Abstract

Alkali metal thermal to electric converter (AMTEC) cells are built with readily available materials. Improvement of the performance of an AMTEC cell requires improvement and development of components as well as cell geometry. The present paper shows parametric results obtained by changing cell geometry to determine the effects of these design changes on the cell performance. In order to improve the cell performance, heat losses, input thermal power, cell's output power and efficiency have been investigated in detail by varying the cell designs. Changing some geometrical dimensions of the cell has proved to be very effective in improving the cell performance. As a result of this overall effort we have been able to demonstrate the improvement in the efficiency of AMTEC cell by 17.5% over the one in operation called Ground Demonstration Converter System at Air Force Research Laboratory, Albuquerque, New Mexico. Published by Elsevier Science S.A.

Keywords: Heat losses; Efficiency; Geometry; Power degradation; AMTEC; Alkali metal

1. Introduction

The alkali metal thermal to electric converter (AMTEC), a direct energy conversion devise, has high conversion efficiency compared with other thermoelectric energy conversion methods. It can theoretically provide efficiency close to the theoretical Carnot efficiency at relatively low temperatures. But efficiencies for AMTEC currently achieved are limited to 15–20%. AMTEC has no moving parts, and therefore no noise or vibration. It is fuel insensitive. It can utilize heat as input fuel from most any source, like fossil fuel, the sun, radioisotopes, or a nuclear reactor. AMTEC, with solar energy as a heat source, is capable of being an alternative to photovoltaic-based power system for use in low earth orbit (LEO) satellites for future NASA and Air Force missions. It is intended to be used for future NASA missions in the millennium 2000 with radioisotope decay as its heat input.

Historically, the concept of AMTEC working was demonstrated in 1968 [1]. The basic operating principle of AMTEC was described by Weber in 1974 [2] and Cole in 1983 [3]. A great deal of interest, however, erupted in AMTEC activities around the world at the beginning of the 1990s. The research and development effort at the Jet Propulsion Lab (JPL) included studies which addressed both overall device construction of the AMTEC components [4–17]. The PX-series cells were designed and manufactured by Advanced Modular Power Systems (AMPS) [18,19] and tested at Air Force Research Lab (AFRL) [20–22]. The use of nuclear power directly from nuclear reactor or radioisotopes based on general-purpose heat source (GPHS) for potential deep space missions has been extensively studied during this period [23–28].

There are several studies about improvement of the cell performance. Schock et al. [29] investigated the effect of several design variables, including cell geometry, on cell performance. The cell was constrained to constant thermal input. El-Genk and Tournier [30] analyzed the effects of various design changes on the performance of next-generation Pluto/Express multi-tube cells. For this, they examined the PX-5A cell with constant hot end temperature by letting the sink temperature vary. Later El-Genk et al. [31] studied different design changes to improve the performance of the PX-3G cell with constant thermal input. Both PX-5A and PX-3G cells have six connected in series BASE tubes of 38.1 mm diameter, PX-5A cell has deep cone evaporator and PX-3G has shallow cone type evaporator. PX-3A has five BASE tubes with 31.75 mm diameter (Table 1).

* Corresponding author. Tel.: +1-806-742-3778; fax: +1-806-742-1182.

E-mail address: b5mak@ttacs.ttu.edu (M.A.K. Lodhi).

[1] Present address: Department of Mechanical Engineering, Karadeniz Technical University, 61080 Trabzon, Turkey.

0378-7753/00/$ - see front matter. Published by Elsevier Science S.A.
PII: S0378-7753(00)00467-5

While these programs successfully resolved a number of key technological issues associated with the successful design and fabrication of AMTEC, the performance level achieved hitherto is still below the theoretical potential of this device. For example, the Carnot efficiency for the PX-3A AMTEC cell with hot end temperature of 1123 K and a condenser temperature of 623 K is 44.5% whereas the achieved efficiency in the laboratory for the same cell was 15% [32]. Moreover, the experimental studies show that the cell performance degrades with the increase of operation time. PX-type AMTEC cells have been tested at AFRL. Merrill and Mayberry [33] have experimentally tested the ground demonstration converter systems (GDCS) of eight cells each of PX-3 and PX-5 AMTEC. The power output for the GDCS decreased by 20.7% over ~3000 h of operation. The experimental data for longer operation time of PX-3A AMTEC cell obtained from AFRL also shows the degradation, see Fig. 1. It is, however, not as much as in the case of GDCS. The test results show that PX-3A AMTEC cell had about 16% degradation in performance in less than 500 h of operation [34]. The PX-3A AMTEC cell is kept at a constant hot end temperature of 1023 K and a condenser temperature of 623 K. This degradation is attributed to the aging of electrodes.

Changing cell materials and/or cell geometry will affect the cell performance. In a recent paper, material parameter analysis shows a marked improvement both in power output and the efficiency of AMTEC cell [35]. In the present paper, we are now investigating the performance of AMTEC PX-3A within the same fixed range of temperature as kept for PX-3A testing at AFRL by modifying its design to overcome some of its degradation. The cell performance can be increased by decreasing the parasitic heat losses. In tracking down the source of power loss during the test cell performance of various AMTEC designs, the major losses are found to be radiative and conductive. Since the cell is tested in vacuum there is no convective loss. The objective of this study is to investigate heat losses depending on geometrical configuration and adjust them to increase the cell performance in a computer simulation to compare with the observed data. For this, we selected the PX-3A AMTEC cell, which has been in operation at the US Air Force Research Laboratory since July 9, 1997.

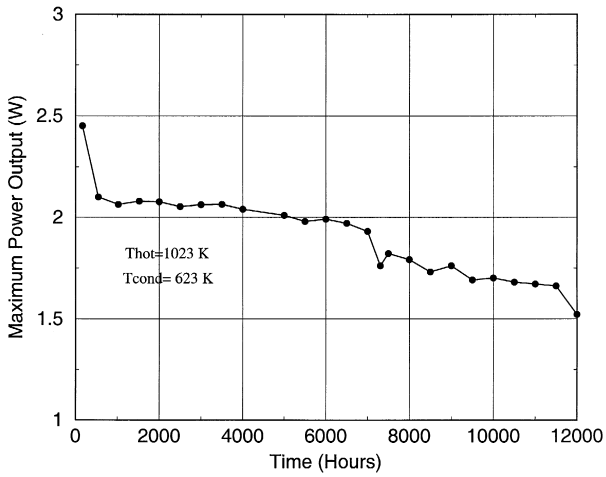

Fig. 1. PX-3A degradation over time.

Table 1
Design parameters of PX-3A cell

Cell diameter (mm)	31.75
Cell height (mm)	101.6
Evaporator type	Deep Cone
Evaporator elevation (mm)	5.18
Evaporator standoff thickness	0.71
Evaporator standoff material	SS
Standoff rings (mm)	1.1
Rings material	Ni
Stud area (mm^2)	38
Stud material	SS
Number of BASE tubes	5
Tube length	32
Electrode/tube (mm^2)	600
Tube braze material	TiNi
Current collector	60-mesh Mo
Feedthrough braze	TiCuNi
Radiation shield type	Circular
Shield material	SS
Condenser type	Creare
Hot side	SS
Cell wall	SS
Initial test date	7/9/97
Operation (h)	12,000

2. AMTEC brief description

An AMTEC cell is a static two-cycle device performing the conversion of heat to mechanical energy via any suitable alkali metal and then the conversion of mechanical energy to electrical energy by utilizing the special properties of the beta″ aluminum solid electrolyte (BASE) material. The general principles governing the operation of an AMTEC cell have been given quite elaborately in the early stages of its development [1–3,36,37]. However, a brief outline is presented here for the self-consistency of this paper. A schematic diagram of a typical AMTEC cell is shown in Fig. 2. A closed vessel is divided into a high temperature, high-pressure region in contact with a heat source and a low temperature, low pressure region in contact with a heat sink separated by a BASE sheet whose ionic conductivity is much larger than its electronic conductivity. The BASE is coated with a porous metal as a cathode that covers the low-pressure surface of the BASE. A closed container is partially filled with a small quantity (typically < 10 g) of liquid sodium as the working fluid.

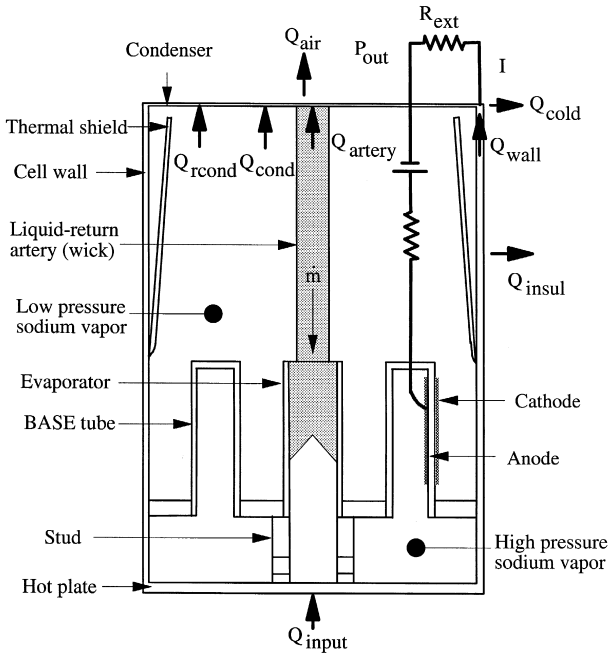

Fig. 2. A schematic diagram of vapor-anode AMTEC cell.

Sodium ions pass through the BASE in response to the pressure differential (gradient of Gibbs free energy). When the circuit is closed electrons flow from the porous anode surface on the high pressure side through the load, producing electrical work to combine with sodium ions to become neutral sodium. The sodium vapor travels to the condenser where it condenses into liquid state. The sodium liquid is pressurized through a wick or electromagnetic pump and is returned to the high-pressure side of the BASE. In that way the thermal-to-mechanical-to-electrical conversion process is completed. The efficiency of this final conversion is governed by a variety of irreversible kinetic and transport processes occurring at the electrode interfaces, within the BASE material, internal impedance, and thermal conduction and radiation losses [4–6].

The transport theory of sodium through an AMTEC cell is rather complicated as it requires the simultaneous solution of thermal, fluid flow, and electrical equations. Those equations are interdependent, through a number of axially varying distribution functions. Specifically, solving for the cell's temperature distribution requires knowledge of the axial variation of the sodium flux through the BASE tube and of the electrical output power density profile over the tube length. Solution of the axial pressure variation of the low-pressure sodium requires knowledge of the cell's temperature distribution and the BASE tubes' current density variation. Similarly, solving for the axial variation of the current density and of the inter-electrode voltage requires prior solution of the axial variation of the BASE tube temperature and internal-to-external pressure ratio. Those interdependent distribution functions require solutions of coupled differential and integral equations that are by no means trivial. In solving these equations some very sophisticated procedures were used, for example, Shock et al. [27] generated a thermal analysis model for multi-tube AMTEC cell by appropriately modifying the ITAS and SINDA codes [38,39].

Energy conversion devices have few equilibria and are typically open systems unlike the classical thermodynamics which is restricted to reversible and closed systems. Onsager's [40] treatment of irreversible processes, such as diffusion, can be applied to AMTEC operations to deal with the irreversibility of the process and openness of the system. One can write, in principle, the effective emf, V as a function of cell voltage in open-circuit, V_{oc} and electrode polarization over potential [2], from the Nernst equation [3] given by:

$$V_{op} = (\zeta^{a} - \zeta^{c}) \quad (1)$$

where ζ^{a} and ζ^{c} are electrode polarization over potentials at anode and at cathode, respectively. The open-circuit voltage and charge-exchange current density are related with the cell temperature and pressure [11]. For the net power output we can write

$$P_{out} = VI, \quad (2)$$

where

$$V = V_{oc} - JR_{int} - V_{op}, \quad (3)$$

$$V_{oc} = RT_{B}/F \ln P_{a}/P_{c}, \quad (4)$$

I is the net current in the circuit and R_{int} is the total internal resistance of the cell including the contact resistance of the electrodes, sheet resistance in the plane of electrodes, resistance of the current collectors, bus wires and conductor leads to the load, the charge exchange polarization losses at the BASE-electrodes interfaces, and the BASE ionic resistance, given by:

$$R_{int} = R_{contact} + R_{sheet} + R_{collector} + R_{bus} + R_{op} + R_{B}. \quad (5)$$

R_{B} is given by:

$$R_{B} = \rho_{B} t_{B}. \quad (6)$$

R is the gas constant = 8.314 J/mol K. The temperature of the BASE tube is T_{B}, P_{a} and P_{c} are the pressures at the anode and cathode sides, respectively, ρ_{B} is the electrical resistivity, the expression for which has been developed by Steinbruck [41], and t_{B} is the thickness of the BASE tube.

In principle, some energy loss in converting heat directly into electricity is inherent, caused in various stages due to several effects. There are some effects that are unavoidable for the AMTEC to work, for example, the latent heat for vaporization and ionization of sodium. The other form of heat losses, however, can be minimized. The AMTEC cell can be assumed as a closed system thermodynamically. For steady-state condition, the thermal energy

entering and leaving through the system boundary and electrical energy produced in the system to be taken into consideration by applying the conservation of energy for the system. For a multi-tube AMTEC cell, the heat transferred on the system is shown in Fig. 2. The total heat loss, Q_{loss} consists of:

$$Q_{loss} = Q_{air} + Q_{insul} + Q_{cold}. \quad (7)$$

Most of the heat passes to the cooling fluid (air), Q_{air}, through the condenser given by

$$Q_{air} = Q_{wall} + Q_{artery} + Q_{rcond} + Q_{cond} - Q_{cold} \quad (8)$$

where Q_{wall} is the conducted heat to condenser through the cell wall, Q_{artery} is conducted heat through the artery, Q_{rcond} is net radiated energy between the condenser and other surfaces, Q_{cond} is the latent heat of condensation of sodium, and Q_{cold} is the heat conduction loss at edge of cold plate. These heat losses can be expressed in the following simplified expressions:

$$Q_{wall} = -k_{wall} A_{wall} (dT/dx)_{x=\text{at condenser}} \quad (9)$$

$$Q_{artery} = -k_{artery} A_{artery} (dT/dx)_{x=\text{at condenser}} \quad (10)$$

$$Q_{cond} = h_{fg} \dot{m} \quad (11)$$

where k is thermal conductivity, A is the area, h_{fg} is latent heat of condensation of sodium per unit mass and $\dot{m}$ is sodium flow rate. dT/dx is the temperature gradient for wall and artery at the condenser. Net radiated energy between the condenser and other surfaces depends on view factors F_{ij}, emissivities ε_i, and temperatures T_i for every surfaces, which can be expressed as

$$Q_{rcond} = f(\varepsilon_1, \varepsilon_2, \varepsilon_3, \ldots, T_1, T_2, T_3, \ldots, F_{11}, F_{12}, F_{13}, \ldots) \quad (12)$$

Some heat goes to ambient through cell wall and insulation; which is given by:

$$Q_{insul} = \int_{x=0}^{x=\text{cell length}} K(x) P [T_{wall}(x) - T_{insul}(x)] dx \quad (13)$$

where $K(x)$ is a constant which includes conduction and radiation effects, and P is the perimeter of cell wall. T_{wall} and T_{insul} are cell wall and insulation temperatures that change along the cell length. Heat conduction loss at edge of cold plate, Q_{cold}, can be calculated similar to Q_{insul} by taking temperature T_{cond} instead of T_{wall}, but Q_{cold} is small. The overall conversion efficiency of AMTEC cell is given by [3,42]:

$$\eta = P_{out}/Q_{input} \cong VI/[VI + Q_{loss}]. \quad (14)$$

In order to get the maximum efficiency the total heat loss, Q_{loss}, must be minimum and P_{out} must be maximum.

3. Procedure

In this study, we have focused on the geometrical configuration of AMTEC. A general examination of the design parameters on cell performance is presented. Several design parameters, such as cell length, cell diameter, stud area, BASE tube length, and electrode length, have been investigated. The geometrical dimensions of various components of the cell have been changed monotonically to study the effect on the power output and the efficiency. The final cell dimensions for all of these cases are given in Table 2. The geometrical configurations for the cell investigated are listed below.

Case A: the length of the cell is increased from 101.6 to 127 mm (25%),
Case B: in addition to case A, the cell diameter is decreased from 31.75 to 26.99 mm (15%),
Case C: in addition to case A, the cell diameter is increased from 31.75 mm to 36.51 mm (15%),
Case D: in addition to case B, the cross-section area of the stud is increased from 37.7 to 120.0 mm^2 (218%),
Case E: in addition to case A, the cross-section area of the stud is increased from 37.7 to 120.0 mm^2 (218%),
Case F: in addition to case D, the length of the BASE tube decreased from 31.75 to 28.58 mm (10%),
Case G: in addition to case D, the length of the BASE tube increased from 31.75 to 36.51 mm (15%), and the

Table 2
Geometrical dimensions for all of the cases

	Cell height (mm)	Cell diameter (mm)	Stud area (mm^2)	Height of BASE tube (mm)	Height of electrodes (mm)
PX-3A	101.60	31.75	37.7	31.75	25.40
Case A	127.00	31.75	37.7	31.75	25.40
Case B	127.00	26.99	37.7	31.75	25.40
Case C	127.00	36.51	37.7	31.75	25.40
Case D	127.00	26.99	120.0	31.75	25.40
Case E	127.00	31.75	120.0	31.75	25.40
Case F	127.00	26.99	120.0	28.58	25.40
Case G	127.00	26.99	120.0	36.51	33.02

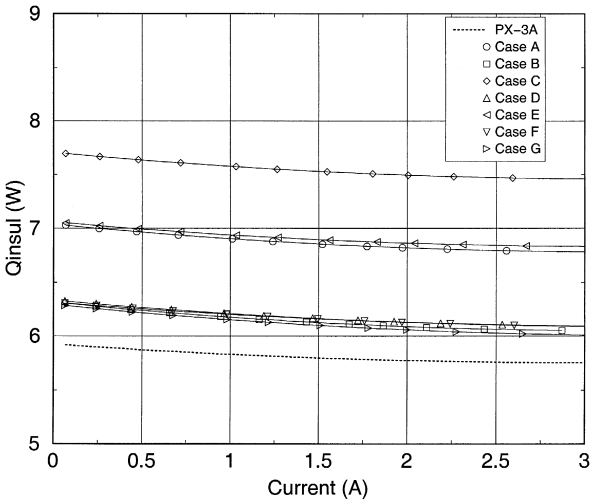

Fig. 3. Heat losses to ambient through cell wall and insulation.

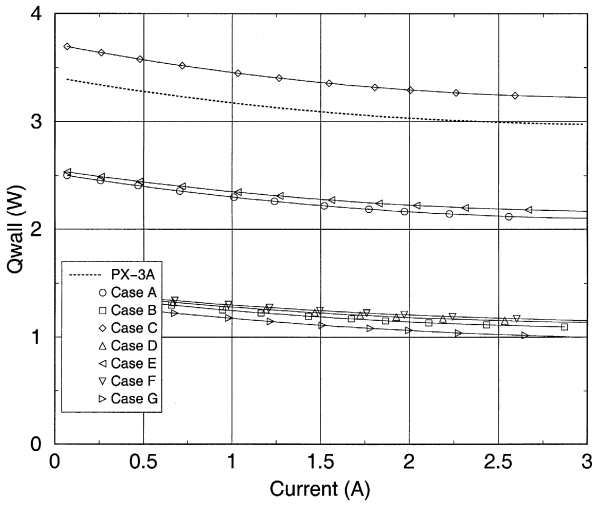

Fig. 5. Conducted heat to condenser through cell wall.

length of the electrodes is increased from 25.40 to 33.02 mm (30%).

4. Results and discussion

Changing the cell dimensions affects the heat losses and the cell performance. It is known that heat conduction depends on cross-section area of, material type, and temperature distribution in the material. Also, thermal radiation is function of surface emissivities, surface areas, surface temperatures, and view factors. If the dimensions of the cell components are changed, some quantities above will take different values and heat losses will be affected in different ways. For example, increasing the cell length will increase Q_{insul} but decrease Q_{rcond}, Q_{wall} and Q_{artery}. For an optimum power output the geometrical parameters of the AMTEC cell have been carefully varied in this work. The effects due to the variation in configuration on the losses from the cell, the amount of the heat supplied to the cell, electrical power generated by the cell, and the efficiency of the cell are given in Figs. 3–9. The hot plate temperature is 1023 K, and the condenser temperature is 623 K for all these cases. In these figures the dotted line corresponds to the configuration of PX-3A AMTEC. The maximum power generated by the cell is given in Table 3. Heat losses are given as the percentage of the Q_{input}. Heat losses through cell wall and insulation, Q_{insul}, through artery, Q_{artery}, and through cell wall, Q_{wall}, are given in Figs. 3–5. As expected, the axial conductive heat losses, Q_{artery} and Q_{wall}, decrease when the length of the cell is increased for case A. Because the thermal resistance increases with increasing conductance length, the temperature gradients at the end of the cell wall and artery take smaller values for larger cell length. But Q_{insul}, in radial

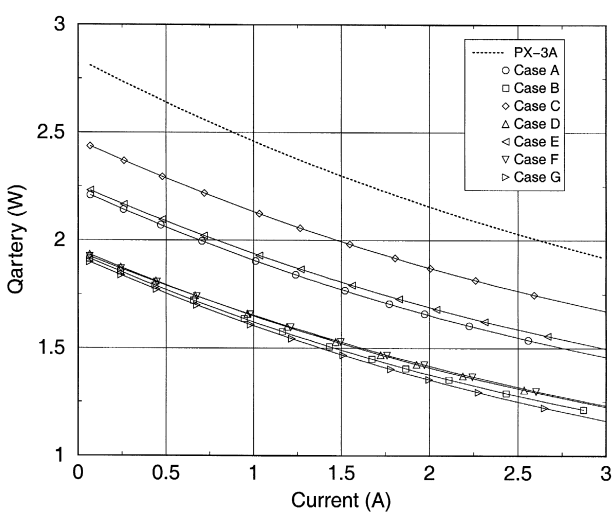

Fig. 4. Conducted heat to condenser through artery.

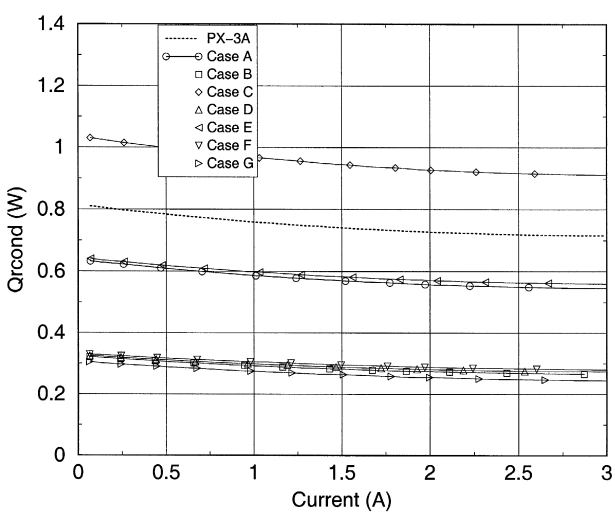

Fig. 6. Radiation heat losses from condenser.

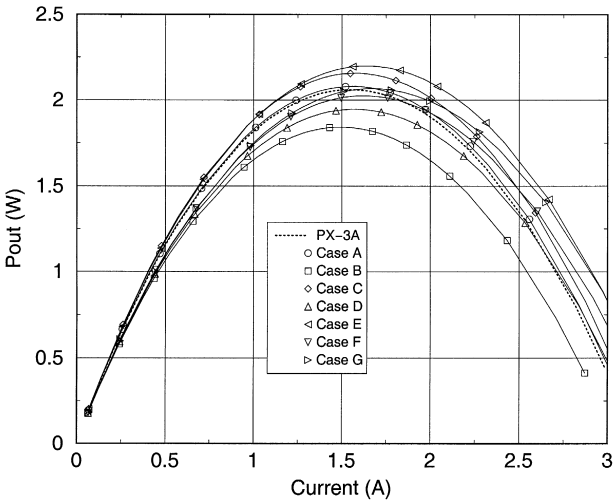

Fig. 7. The electrical power generated by the cell.

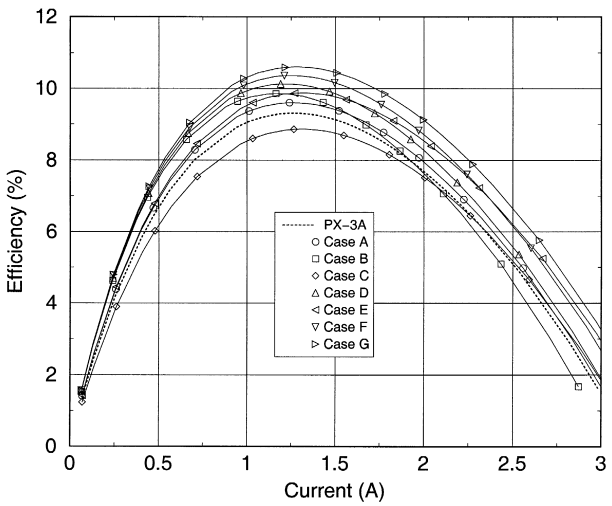

Fig. 9. The cell conversion efficiency.

direction, increases because of larger cell wall surface area. For case B (smaller cell diameter), Q_{insul}, Q_{artery} and Q_{wall} decrease and take the smallest value for all the cases. The smaller cell diameter causes the hot plate surface area to become smaller, thus Q_{input} decreases. All heat losses, which depend on Q_{input}, are also least. On the contrary, when the cell diameter is increased, in case C, the conductive heat losses, Q_{insul}, Q_{artery} and Q_{wall}, increase. In cases D and E, the situations of larger cross-section of stud, more heat passes into the cell through the hot plate at the same hot plate temperature, Fig. 8. Therefore, heat losses increase, compared with the smaller cross-section area of stud cases (A and B), Figs. 3–5. Also, heat losses change with length of the BASE tube and length of the electrodes, in cases F and G. In Fig. 6, the net heat radiation to condenser, Q_{rcond}, is given as a function of current. It shows similar pattern to Q_{wall} as in Fig. 5. For all cases, Q_{insul} shows higher values than at PX-3A cell, but Q_{artery} gives smaller values. Also the values of Q_{wall} and Q_{rcond} are smaller for all cases except C.

For all cases, the electrical power generated by the cell, P_{out}, the amount of heat supplied to the cell, Q_{input}, and the cell conversion efficiency are given in Figs. 7–9, respectively. For case C of increased cell diameter the cell conversion efficiency decreases, although P_{out} increases by 4.85% against PX-3A cell, because Q_{input} increases by 9.55%. When the diameter of the cell is reduced, cases B and D, P_{out} becomes smaller against PX-3A cell, and so does Q_{input}. However, since the Q_{input} decreases more than P_{out} the cell conversion efficiency increases, as in those seen in Figs. 6–9. Using a larger cross-section area of stud increases P_{out} and the cell efficiency. When length of BASE tube is decreased from 31.75 to 28.58 mm, in cases F and D, it is seen that the cell efficiency and P_{out} increase. In case G, as the length of the electrode is increased (for this, length of the BASE tube is also in-

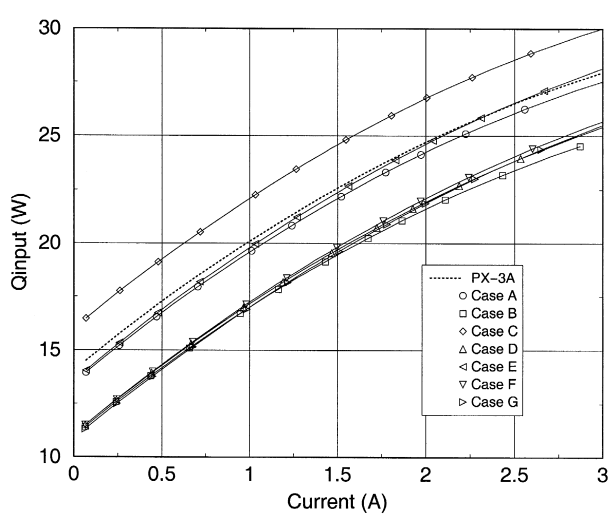

Fig. 8. The heat supplied to the AMTEC cell.

Table 3
Maximum power generated, current, efficiency and heat losses by the AMTEC cell

	PX-3A	Case A	Case B	Case C	Case D	Case E	Case F	Case G
$P_{out,max}$ (W)	2.06	2.08	1.84	2.16	1.95	2.20	2.02	2.07
I (A)	1.56	1.56	1.47	1.59	1.56	1.66	1.59	1.66
η (%)	9.02	9.29	9.53	8.64	9.76	9.52	9.97	10.17
Q_{input} (W)	22.83	22.38	19.33	25.01	19.98	23.11	20.26	20.35
Q_{insull} (W)	5.79	6.85	6.13	7.52	6.16	6.88	6.15	6.08
Q_{insull} (%)	25.36	30.61	31.71	30.07	30.83	29.77	30.36	29.88
Q_{artery} (W)	2.28	1.75	1.50	1.97	1.51	1.77	1.51	1.43
Q_{artery} (%)	9.99	7.82	7.76	7.88	7.56	7.66	7.45	7.03
Q_{wall} (W)	3.08	2.21	1.19	3.35	1.22	2.26	1.24	1.09
Q_{wall} (%)	13.49	9.87	6.16	13.39	6.11	9.78	6.12	4.91
Q_{rcond} (W)	0.74	0.57	0.28	0.94	0.29	0.58	0.29	0.26
Q_{rcond} (%)	3.24	2.55	1.45	3.76	1.45	2.51	1.43	1.28
Q_{cond} (W)	8.64	8.68	8.16	8.83	8.62	9.17	8.79	9.16
Q_{cond} (%)	37.84	38.78	42.21	35.31	43.14	39.68	43.39	45.01

Table 4
Comparison of maximum conversion efficiency of the AMTEC cell

	PX-3A	Case A	Case B	Case C	Case D	Case E	Case F	Case G
I (A)	1.24	1.24	1.16	1.32	1.19	1.33	1.27	1.28
η_{max} (%)	9.03	9.60	9.86	8.86	10.12	9.87	10.36	10.61
Improvement in efficiency (%)	–	6.31	9.19	−1.88	12.07	9.30	14.73	17.50
P_{out} (W)	1.98	2.00	1.76	2.11	1.84	2.13	1.94	1.96

creased), P_{out} and the cell efficiency also increased, see Tables 2–4.

5. Conclusion

The cell weight change depends on its geometrical dimensions. We did not want to increase the cell weight too much. Making several small changes in the cell dimensions provided up to 17.50% improvement in conversion efficiency of AMTEC cell. The following observations are worth noticing:

- As the cell height increases the conversion efficiency and the maximum electrical power generated are increased within the range considered.
- The larger cell diameter decreases cell conversion efficiency, but increases the maximum electrical power generated by the cell.
- The larger cross-section of stud increases both cell conversion efficiency and the maximum electrical power generated by the cell.
- When length of the electrode is increased, both cell conversion efficiency and the maximum electrical power generated by the cell increase.

List of symbols

A_{artery}	cross-section area of artery (m^2)
A_{wall}	cross-section area of wall (m^2)
F	Faraday's constant (96,485 C/mole)
F_{ij}	view factor between surfaces i and j
h_{fg}	latent heat of condensation of sodium per unit mass (J/kg)
I	cell current (A)
J	current density (A/m^2)
k	thermal conductivity (W/mK)
K	coefficient includes conduction and radiation effects (W/mK)
$\dot{m}$	sodium flow rate (kg/s)
P	perimeter of cell wall (m)
P_a	pressure at anode side (Pa)
P_c	pressure at cathode side (Pa)
P_{out}	electrical energy generated by the cell (W)
Q_{air}	heat passes the air as cooling fluid (W)
Q_{artery}	conducted heat to condenser through artery (W)
Q_{cold}	heat loss at the edge of cold plate (W)
Q_{cond}	latent heat of condensation of sodium (W)
Q_{insul}	heat losses to ambient through cell wall and insulation (W)
Q_{loss}	total heat losses (W)
Q_{rcond}	net radiated energy to condenser (W)
Q_{wall}	conducted heat to condenser through cell wall (W)
R	perfect gas constant (8.314 J/mol K)
R_{bus}	electrical resistance of bus wire (Ω m^2)
R_B	ionic electrical resistance (Ω m^2)
$R_{collector}$	electrical resistance of current collector (Ω m^2)
$R_{contact}$	contact resistance of the electrodes (Ω m^2)
R_{int}	total internal resistance (Ω m^2)
R_{op}	charge exchange polarization loss (Ω m^2)
R_{sheet}	sheet resistance in the plane of electrode (Ω m^2)
t_B	thickness of BASE tube (m)
T	temperature (K)
V	Cell voltage (V)
V_{oc}	cell voltage in open-circuit (V)
V_{op}	electrode polarization over potential (V)
x	distance from condenser (m)

Greek

ε	emissivity
η	cell conversion efficiency
ρ_B	electrical resistivity (Ω m)
ζ^a	electrode polarization over potential at anode (V)
ζ^c	electrode polarization over potential at cathode (V)

Acknowledgements

We are indebted to Clay Mayberry and John Merril for providing the AMTEC data before publication and Dr. Jean-Michel Tournier for many useful discussions. This work is based in part upon work supported by the Center for Energy Research, Texas Tech University and Texas Advanced Technology Program under Grant Number 003644-091, and AFOSR Sub-contract 99-0832 CFDA #12.800.

References

[1] J.T. Kummer, N. Weber, U.S. Patent 3,458,356, assigned to Ford Motor Co. (1968).
[2] N. Weber, Energy Convers. 14 (1974) 1.

[3] T. Cole, Science 221 (1983) 915.
[4] R.M. Williams, B. Jeffries-Nakamura, M. Underwood, B. Wheeler, M. Loveland, S. Kikkert, J. Lamb, T. Cole, J. Kummer, C.P. Bankston, J. Electrochem. Soc. 136 (1989) 893.
[5] R.M. Williams, M.E. Loveland, B. Jeffries-Nakamura, M.L. Underwood, C.P. Bankston, H. Leduc, J.T. Kummer, J. Electrochem. Soc. 137 (1990) 1709.
[6] R.M. Williams, B. Jeffries-Nakamura, M.L. Underwood, C.P. Bankston, J.T. Kummer, J. Electrochem. Soc. 137 (1990) 1716.
[7] M.A. Ryan, B. Jeffries-Nakamura, R.M. Williams, M.L. Underwood, D. O'Connor, S. Kikkert, Proc. 26th Intersociety Energy Conversion Engineering Conference, Am. Nucl. Soc. 51991, p. 463.
[8] M.A. Ryan, R.M. Williams, B. Jeffries-Nakamura, M.L. Underwood, D. O'Connor, JPL New Technology Report, 18620-8166 (1991) .
[9] M.A. Ryan, B. Jeffries-Nakamura, D. O'Connor, M.L. Underwood, R.M. Williams, Proc. Symposium on High Temperature Electrode Materials and Characterization, in: D.D. Macdonald, A.C. Khanker (Eds.), Electrochem. Soc. vol. 91-61991, p. 115.
[10] C.B. Vinning, R.M. Williams, M.L. Underwood, M.A. Ryan, J.W. Suiter, Proc. 27th Intersoc. Energy Convers. Eng. Conf. 3 (1992) 123, Society of Automobile Engineers.
[11] M.L. Underwood, R.M. Williams, M.A. Ryan, B. Jeffries-Nakamura, D. O'Connor, in: M.S. El-Genk, M.D. Hoover (Eds.), Proc. 9th Symp. Space Nucl. Power Syst. vol. 31992, p. 1331, American Institute of Physics.
[12] M.L. Underwood, D. O'Connor, R.M. Williams, B. Jeffries-Nakamura, M.A. Ryan, Proc. 27th IECEC 3 (1992) 197.
[13] M.L. Underwood, B. Jeffries-Nakamura, D. O'Connor, M.A. Ryan, J.W. Suitar, R.M. Williams, Proc. 28th IECEC 1 (1993) 855.
[14] M.A. Ryan, R.M. Williams, B. Jeffries-Nakamura, M.L. Underwood, D. O'Connor, NASA Tech. Briefs (1993) 80.
[15] M.A. Ryan, R.M. Williams, C. Spaipetch, A. Kisor, D. O'Connor, M.L. Underwood, B. Jeffries-Nakamura, CONF940101, AIP Press, New York, 1994, p. 1495.
[16] M.A. Ryan, A. Kisor, R.M. Williams, B. Jeffries-Nakamura, D. O'Connor, Proc. 29th IECEC 2 (1994) 877.
[17] M.A. Ryan, R.M. Williams, M.L. Phillips, L. Lora, J. Miller, in: M.S. El-Genk (Ed.), Proc. Space Technology and Applications International Forum, AIP Press, New York, 1998, p. 1607.
[18] R.K Sievers, T.K. Hunt, J.F. Ivanenok, J. Pantolin, D.A. Butkiewicz, in: M.S. El-Genk, M.D. Hoover (Eds.), Proc. 10th Space Nuclear Power and Propulsion, CONF-930103, AIP Press, New York, 1993, p. 319.
[19] R.K. Sievers, J.R. Rasmussen, C.A. Barkowski, T.J. Hendricks, J.E. Pantolin, Proc. STAIF-98, CONF-980103, AIP Press, New York, 1998, p. 1479.
[20] M.J. Schuller, P. Haugen, E. Reiners, J. Merrill, R.K. Sievers, R. Svedberg, J.F. Ivanenok III, C.J. Crowley, M.G. Izenson, Proc. 31st IECEC, IEEE, paper no. 96184 2 (1996) 877.
[21] J. Merrill, M.J. Schuller, R.K. Sievers, C.A. Borkowski, L. Huang, M.S. El-Genk, Proc. 32nd IECEC, IEEE, paper no. 97379 2 (1997) 1184.
[22] J.M. Merrill, M. Schuller, L. Huang, Proc. STAIF, in: M.S. El-Genk (Ed.), CONF-980103, AIP Press, New York, 1998, p. 1613.
[23] A. Shock, Proc. 15th Intersociety Energy Conversion Engineering Conference vol. 2 AIAA, New York, 1980, p. 1032.
[24] D. Birden, F.A. Angelo, Proc. 18th Intersociety Energy Conversion Engineering Conference, AICHE, New York, 1983, p. 61.
[25] E.J. Brat, G.O. Fitzpatrick, Direct Conversion Nuclear Reactor Space Power Syst., Report No. AFWALTR-82-2073, vol. 1.
[26] A. Schock, Proc. 15th Intersoc. Energy Convers. Eng. Conf. (1980) 1032.
[27] A. Schock, H. Norivan, C. Or, V. Kumar, Proc. 48th Intl. Astron. Congr. (1997) 1.
[28] A. Schock, H. Norivan, C. Or, V. Kumar, Preprint for presentation in 33rd Intersoc. Energy Convers. Eng. Conf. (1998).
[29] A. Schock, H. Noravian, V. Kumar, C. Or, Proc. 32nd Intersociety Energy Conversion Conf., # 97529 2 (1997) 1136.
[30] M.S. El-Genk, J.M. Tournier, 15th STAIF, AIP Press, New York, 1998, p. 1461.
[31] M.S. El-Genk, J.M. Tournier, R. James, C. Mayberry, 16th STAIF, AIP Press, New York, 1999, p. 1293.
[32] M.S. El-Genk, J-M. Tournier, Proc. 5th ESPC-98 416 (1998) 257.
[33] J.M. Merrill, C. Mayberry, 16th STAIF, AIP Press, New York, 1999, p. 1369.
[34] J.M. Merrill, M. Schuller, L. Huang, 15th STAIF, AIP Press, New York, 1998, p. 1613.
[35] M.A.K. Lodhi, A. Daloglu, J. Power Sources, in press.
[36] T.K. Hunt, N. Weber, T. Cole, Proceeding of the 13th Intersociety Energy Conversion Engineering Conference, SAE, Warrandale, PA, 1978, p. 2001.
[37] K. Hunt, N. Weber, T. Cole, in: J.B. Bates, G.C. Ferrington (Eds.), Solid State Ionics, North Holland, Amsterdam, 1981, p. 263.
[38] H. Noravian, Proc. 26th Int. Conference on Environmental Systems, No. 961376 (1996) .
[39] J. Gaski, SINDA (System Improved Numerical Differencing Analyzer), ver. 1.315 from Network Analysis Associate, Fountain Valley, CA, 1987.
[40] L. Onsager, Phys. Rev. 38 (1931) 2265.
[41] M. Steinbruck, V. Heinzel, F. Huber, W.M. Peppler, Proc. 28th IECEC I 1 (1993) 799.
[42] C.J. Crowly, M.G. Izenson, P.N. Wallis, R.K. Sievers, J.F. Ivanenok III, Proc. 29th IECEC vol. 1 AIAA, 1994, p. 882.